Tannin-furanic foams modified by soybean protein isolate (SPI) and industrial lignin substituting formaldehyde addition

Xinyi Chen, Jinxing Li, Antonio Pizzi, Emmanuel Fredon, Christine Gerardin, Xiaojian Zhou, Guanben Du

Tannin-Furanic Foams Modified by Soybean Protein Isolate (SPI) and Industrial Lignin Substituting Formaldehyde Addition

Xinyi Chen[1,2†], Jinxing Li[1†], Antonio Pizzi[2]*, Emmanuel Fredon[2], Christine Gerardin[3], Xiaojian Zhou[1]*, Guanben Du[1]

1 Key Laboratory for Forest Resources Conservation and Utilisation in the Southwest Mountains of China (Southwest Forestry University), Ministry of Education, Kunming 650224, PR China

2 LERMAB, University of Lorraine, 27 rue Philippe Seguin, BP 1041, 88051 Epinal, France

3 LERMAB, University of Lorraine, Boulevard does Aiguillettes, 54000 Nancy, France

* Corresponding Author: Antonio PIZZI. Tel.: +33-623126940. E-mail address: antonio.pizzi@univ-lorraine.fr;

Xiaojian ZHOU. Tel.: +86-187 2527 6030. E-mail address: xiaojianzhou@hotmail.com

† These authors contributed equally to this work

Abstract:

Soybean protein isolate (SPI) was tested in this study as a crosslinker and formaldehyde substitute for preparing high biomass content sustainable rigid tannin-furanic-SPI (TFS) and lignin-tannin-furanic-SPI (LTFS) versatile foams. Additionally, flame retardancy was improved by lignin used as a natural fire-retardant. Fourier-transform infrared spectroscopy (FT-IR), coupled with matrix-assisted laser desorption/ionization time-of-flight mass spectrometry (MALDI-ToF-MS), revealed a covalent cross-linking reaction between tannin and SPI. TFS and LTFS foams showed by scanning electron microscopy (SEM) a closed cell structure without any pores. The incorporation of SPI resulted in enhanced mechanical properties and reduced pulverization ratios, improved thermal stability and increased thermal conductivity (approximately 0.042–0.044 W/m·K) compared with control foam. Furthermore, the TFS foams exhibited outstanding flame retardancy and suppressed smoke generation while undergoing combustion. These results were supported by a higher limiting oxygen index (LOI) value, a lower heat-release rate, and a higher char residue, obtained by LOI and cone calorimetry. The addition of lignin further enhanced the thermal properties and flame retardancy of TFS foams although it decreased their mechanical performance. The TFS and LTFS foams were environmentally friendly, as shown by the low formaldehyde emission measurements. This novel sustainable TFS foam appears to have a good potential for industrial application.

Key words:

Mimosa tannin, SPI, Sustainable rigid foam, Limiting oxygen index (LOI), Flame retardancy

1 Introduction

Sought-after characteristics, such as flame retardancy, better thermal stability, lightweight, and thermal insulation, are found in phenolic foam (PF). Yet PF has high friability and inferior mechanical properties and is a fossil fuel-based resource, which limits somewhat its large-scale commercial applications (Chen et al., 2020a; Wu et al., 2020). Therefore, foams with improved mechanical properties using natural renewable feedstocks have attracted much attention. Condensed tannin—a vegetal polyphenolic material which is widespread—has been applied in several field (Chen et al., 2020a; Meikleham and Pizzi, 1994; Pizzi, 2019).

Phenolic tannin-furanic-formaldehyde foams were first reported by Meikleham and Pizzi in 1994 and have since received significant attention (Meikleham and Pizzi, 1994; Pizzi, 2019). The interest of these foams is not only because they are based on a renewable resource but also because of theirs self-blowing preparation under ambient/moderate temperature, and their comparable performance with commercial PF foams (Meikleham and Pizzi, 1994; Pizzi, 2019; Tondi and Pizzi, 2009; Tondi et al., 2008a; Tondi et al., 2009c; Zhou et al., 2019).

The preparation approaches for these foams are based on a heat-generated expansion initiated by a blowing agent evaporation coupled with an acid-catalysis self-condensation of furfuryl alcohol, without (Basso et al., 2011) or with a cross-linker ensuring the foam structure does not collapse (Celzard et al., 2010; Tondi et al., 2009b; Tondi and Pizzi, 2009; Tondi et al., 2008a; Tondi et al., 2009c; Zhou et al., 2019). Various foams have been obtained for different application fields, such as rigid, semi-rigid, and flexible foams via formulation and/or processing adjustment (Basso et al., 2014a; Basso et al., 2014b; Basso et al., 2011; Celzard et al., 2011; Celzard et al., 2010; Lacoste et al., 2013; Li et al., 2012c; Meikleham and Pizzi, 1994; Pizzi, 2019; Tondi et al., 2009a; Tondi et al., 2009b; Tondi and Pizzi, 2009; Tondi et al., 2008a; Tondi et al., 2009c; Zhou et al., 2019). Yet, because of their brittleness they powder easily on frictioning them and present lower mechanical compression properties, these foams have limited commercial application. Their susceptibility to powdering under friction has been solved well (Rangel et al., 2016). However, to reduce the foam brittleness and to enhance other properties (flame retardancy, thermal stability, and thermal insulation) so as to achieve their industrialization, some improved formulations have been developed by introducing organic/inorganic additives, such as polymeric diphenylmethane

diisocyanate (p-MDI) (Li et al., 2012a), hyperbranched poly(amino-ester) (Li et al., 2012b), multi-walled carbon nanotubes (Li et al., 2013), disordered carbon matrix and graphite fillers (Jana et al., 2015), cellulose nanofibers (CNF) (Zhou et al., 2019), wood cellulosic fiber(Wu et al., 2020), hydroxy-methylated lignin (Pizzi, 2019) and boric and/or phosphoric acid (Celzard et al., 2011). Formaldehyde-free modifications have been introduced early on to take into account human health and the environment. Thus, formulations with no aldehydes at all (Basso et al., 2013; Basso et al., 2011), or with non-toxic and non-volatile aldehydes such as glyoxal and glutaraldehyde (Lacoste et al., 2013), or fossil-based resources such as PEG-400 and polymeric diphenylmethane diisocyanate (p-MDI) (Li et al., 2012a), and biorefinery byproduct such as polyfuranic humins (Chen et al., 2020a) have been reported as the part of feedstocks that can replace formaldehyde to produce tannin-furanic foams. Mechanical or/and chemical expansion methods have also been utilized to prepare tannin-based rigid foams with lower density, thermal insulation, and robust cell structure (Santiago-Medina et al., 2018a; Santiago-Medina et al., 2018b; Szczurek et al., 2014).

Plant or animal proteins have also attracted attention for their successful utilization for bio-foams preparation. Albumin was initially used to design and manufacture flexible biofoams (Basso and Pizzi, 2017; Basso et al., 2015; Li et al., 2012c; Li et al., 2012d) with a series of different natural albumin and albumin/tannin cellular foams following (Basso and Pizzi, 2017; Basso et al., 2015; Lacoste et al., 2015). Biomass foams based on wheat gluten have also been reported (Chiou et al., 2020). However, soy flour and soy protein isolate (SPI) are plant-sourced, renewable, sustainable, and easily obtained from soybean-oil production processing, which is why it has been a commonly applied bioresource for the food industry (Guo et al., 2018; Ma et al., 2020), film preparation (Cao et al., 2007; Gu et al., 2019; Wang et al., 2017), in biomedicine (Zhao et al., 2018), and for wood adhesive applications (Liu et al., 2017; Zhao et al., 2018). SPI was once the main raw material or reinforcement filler for different kinds of foam design (Frihart and Lorenz, 2019; Frihart et al., 2019; Liu et al., 2017; Liu et al., 2015; Wang et al., 2019; Xi et al., 2020; Xiao et al., 2013; Zhao et al., 2019). This encouraged us to design and investigate SPI for tannin-furanic foam preparation because of the reputed reaction crosslinking reaction between tannin and SPI (Ghahri et al., 2018a; Ghahri and Pizzi, 2018; Ghahri et al., 2018b; Liu et al.,

2017) as only a small amount of SPI addition can achieve unexpected effectiveness.

Thus, here are presented novel mimosa tannin-furanic-SPI (TFS) and lignin-tannin-furanic-SPI (LTFS) versatile foams. Lignin was selected as the natural flame-retardant to improve the flame retardancy of the-resultant TFS foams. The reaction between tannin and SPI was examined. The combined properties of the control, TFS, and LTFS foams, including apparent density, morphology, pulverization ratios, and mechanical properties, were systematically evaluated. Furthermore, the thermal stability, thermal conductivity, and especially fire retardancy of the foams were investigated. The formaldehyde emission of the foams obtained was determined to further demonstrate its environment-friendly characteristics.

2 Materials and methods

2.1 Materials

Commercial mimosa tannin extract (*Acacia mearnsii, De Wild,* its main components as shown in Table S1) was provided by Silva Chimica (St. Michele Mondovi, Italy). Soy protein isolate (SPI) was purchased from Ruikang Biotechnology Co., LTD (Dezhou, China). Lignin was obtained from Anhui BASF Biotechnology Co. LTD (Anhui, China). Furfuryl alcohol (FA, 98%), Formaldehyde (F, 37%), p-toluene-4-sulfonic acid (p-TSA, 65%) and Diethyl ether (DE, 98%) were purchased from Sigma-Aldrich (Saint Louis, France). All materials and chemicals used the experiments were employed directly without further treatment.

2.2 Preparation of tannin-based foams

This research reported tannin-based foams were prepared according to the formulation showed in Table 1. The control foam was obtained according to reference (Zhou et al., 2019) and the principle originally presented in reference (Meikleham and Pizzi, 1994). In brief, tannin extract was mixed with furfuryl alcohol thoroughly. A certain amount of deionized water (as shown in Table 1) was added into the mixture and stirred intensely for 10 s. A mixture solution containing formaldehyde and p-TSA was added to the tannin and furfuryl alcohol mixture and stirred for 5 s. The blowing agent diethyl ether was added into the mixture and then stirred for 20 s till to obtain a homogenous slurry. The product was placed in an oven for foaming and aging for at 24 h. The resulting black foam was obtained and labeled as the control.

The TFS and LTFS foams were prepared following the control sample processes, as outlined in

Table 1. The SPI or lignin/SPI mixture was used to substitute for formaldehyde completely. The SPI addition amount in TFS and LTFS foams depended on the formaldehyde solid content of the control. In parallel, the results of pre-experiments showed that 1–4 g SPI and 0.5–2 g lignin were appropriate. The resultant foams without lignin were labelled as TFS and the foams with lignin were labelled as LTFS. All resulting foams were stored under ambient conditions for at least two days before sample preparation and testing.

[Table 1 near here]

2.3 Foam characterization

The apparent densities of the foams prepared were checked according to the ASTM D1622-03 standard (Li et al., 2019). The foam dimensions were 30 × 30 × 30 mm. Five repeated trials were conducted to calculate the mean values and standard deviations.

The foam morphology was observed by scanning electron microscopy (SEM, Hitachi TM-3000, Milexia, Paris, France) under the acceleration voltage of 15 kV. To increase the electric conductivity of samples, a thin gold coating process was conducted before measuring.

Fourier-transform infrared spectroscopy (FT-IR, PerkinElmer Frontier ATR-FTMIR) was utilized to investigate the functional groups during the foam preparation. Each sample were recorded with 32 scans between the wave range of 600 and 4000 cm^{-1}, with a scan resolution of 4 cm^{-1}.

Matrix-assisted laser desorption/ionization time-of-flight mass spectrometry (MALDI-ToF-MS, AXIMA Performance, Shimadzu, Manchester, UK) was adopted to detect products-derived from the reaction between tannin and SPI. The measurements were carried out making 1000 profiles per sample with two shots accumulated per profile. The spectrum precision was of ±1 Da (Jahanshahi et al., 2016).

The viscosity of foaming resin precursor was tested with a Brookfield DV-II+ Viscometer, chose spindle No. 4 at 12 rpm under ambient environmental conditions.

The pulverization ratios were evaluated following the reference (Li et al., 2021). The samples were cut to the uniform size of 50 × 50 × 50 mm. The repeat experiments were performed five times.

The compression strengths were carried out by using the universal testing machine (Instron 3300,

Elancourt France) with a foam dimension of 30 × 30 × 30 mm (Chen et al., 2020b). Each experiment's average value was from the three repeated measurements.

Thermal conductivity experiments were performed under ambient conditions by using a YBF-2 apparatus (Dahua Ltd., Hangzhou) with the foam slice radius 50 mm and thickness 10 mm, according to the method reported by references (Li et al., 2019; Zhou et al., 2019). Three repeated experiments were conducted, and we report the average and standard deviations.

Thermogravimetry analysis (TGA) was carried out using a TGA5500 analyzer (TA Instruments, USA). The measurements of foams were made between 25℃ and 790℃ with a heating rate of 10℃/min under nitrogen atmosphere.

Limiting oxygen index (LOI) measurements of samples were conducted based on the China National Standards GB/T 2406.2-2009 utilizing XWR-2046 oxygen index apparatus (Yilu Instrument Co., LTD, Changzhou, China) (Li et al., 2019). The size of samples was 80 × 10 × 10 mm for testing. The average value and standard deviations were obtained from five experiments trials.

A cone calorimeter (CC, FTT, UK) was used to estimate the combustion behavior of the control, TFS and LTFS samples according to ISO 5660 standards (Kong et al., 2018). The size of the samples was 100 × 100 × 50 mm. The testing was carried out under a heat flux of 35 kW/m^2.

The formaldehyde emission was tested according to China National Standards GB/T 17657-2013. The samples were pre-balanced at 65% humidity and 20℃ at least 7 days before testing. Three repeated trials were conducted.

3 Results and discussions

3.1 The preparation of tannin-furanic-SPI foams

The fabrication of versatile tannin-furanic-SPI foams with high biomass content (~88%) derived from natural lignocellulosic biomass-derived products (furfuryl alcohol and tannin) and a sustainable soybean derivative (SPI) is schematically illustrated in Figure 1. This formulation avoided the toxic formaldehyde utilization, improving the fabrication safety and environmentally friendly nature of the foams with enhanced properties.

There are a number of simultaneous reactions occurring, as described by MALDI-ToF-MS analysis in this work, and they contribute to the expansion of the foams and to their stability of

crosslinking. The furfuryl alcohol self-condensation exotherm accelerated the evaporation of the blowing agent, resulting in a volume expansion of the resultant foam. Furfuryl alcohol not only links to the tannin, but also reacts with the amino groups of the amino side-chains of SPI, namely of arginine. The MALDI-ToF-MS analysis confirmed the formation of such covalent bonds. In addition, esterification of the carboxylic acids side-chain of SPI, aspartic and glutamic acid, also probably occurs with the tannin flavonoid units alcoholic C3 hydroxyl groups and possibly also with its phenolic hydroxyl groups. Ionic bonds between the same groups, that are also known to occur at ambient temperature between soy protein and tannin (Ghahri et al., 2018a; Ghahri and Pizzi, 2018; Ghahri et al., 2018b) reduce drastically under the action of a higher temperature. Thus, the three-dimensional structure of the foams was obtained and maintained also by the additional cross-linking engendered by the interaction between tannin and SPI.

The contributing function of the crosslinker in this reaction processing was confirmed. The experimental results showed that the volume expansion reached a maximum and then shrank with the collapse of the cellular structure. As shown in Figure S1, the homogeneous, dark, and rigid control, TFS, and LTFS foams were obtained.

[Figure 1 near here]

3.2 The suggested reaction mechanism between tannin and SPI

3.2.1 MALDI-ToF-MS analysis

The MALDI-ToF-MS spectra reported in the literature indicate that under the conditions used not only there are the reactions of furfuryl alcohol self-polymerization (Tondi et al., 2008b), furfuryl alcohol with the tannin (Abdullah and Pizzi, 2012; Pizzi et al., 2008), and furfuryl alcohol with the amino groups of the side chains of the protein (Liang et al., 2017), but that there are also reactions that occur between the tannin and SPI without any intervention of other compounds. It is for this reason that a MALDI-ToF-MS analysis of the reaction of tannin with SPI alone under the same conditions used for the foam was carried out, the corresponding spectra being summarized in Figure 2 (a) – (c).

These MALDI-ToF-MS spectra showed that tannin and aminoacids such as arginine presenting amino groups on their side chain do react by substituting some of the hydroxyl groups of the tannin linking it to the protein, as shown in Table 2 (a). This amination reaction of tannin is

212 known and used, for instance, with ammonia (Braghiroli et al., 2013; Santiago-Medina et al.,
213 2017; Thébault et al., 2017). Also, esterification reactions of the alcoholic and possibly even of
214 the phenolic -OH groups of the tannin with the carboxylic acid function of the side chain of other
215 amino acids, such as aspartic acid or glutamic acid do occur as shown in Table 2 (b) and (c).
216 Thus, mono flavonoids reacted with a single aminoacid, such as fisetinidin-leucine, with the
217 flavonoid in both its normal and its open form as at 410 Da, and at 390 Da do occur, their
218 corresponding structures being summarized in Table S2.
219 Although several such compounds are found in the spectra, they do not contribute to the tannin
220 and protein cross-linking because once the amino acid is not free but linked within the skeletal
221 peptide chain of the protein the amino group is changed to an amide, and the -NH- amide group
222 is less likely to react with the tannin (both for its lower reactivity and for the steric hindrance
223 engendered). Thus, the amination of the tannin can occur only through amino acids with amino
224 or imino groups on the side chains of the protein. In soy these are arginine, lysine and proline.
225 The existence of this reaction is then proved by the reaction of tannin monomers and dimers with
226 peptides containing one of these three aminoacids, such as the structure represented by the series
227 of peaks at 857 Da, 873.1 Da, 889.2 Da, 1128.1 Da, 1144.1 Da, 1162 Da, 1177.4 Da, 1193.5 Da,
228 1260.5 Da, 1450 Da, and 1466 Da which are presented in Table S2. The latter one of these, for
229 example, is a catechin-fisetinidin flavonoid dimer linked on one site to a peptide fragment of four
230 amino acids, arginine-leucin-aspartic acid-tryptophan, through the side chain -NH_2 of arginine,
231 but also linked and linked to a second peptide chain fragment formed by tryptophan-aspartic acid
232 in which the free -NH_2 not converted to skeletal amide of one of the two amino acids has reacted
233 with the flavonoid dimer too, thus a structure as of the type in Table 2 (d).
234 To illustrate, as an example, the possibility that the reaction of the protein with the flavonoid
235 units of the tannin can occur either through the amino group of a protein side chain or by
236 esterification with the acid group of a side chain of the protein, the peak at 1260 Da can be
237 brought as an example (Table 2 (e) and (f)).
238 It must be considered that in the case of the structure assigned to the 1260 Da peak (Table 2 (f)),
239 esterification is most likely to occur first at the alcoholic -OH on the flavonoids C3 before
240 occurring on the more acid phenolic -OH groups. The assigned compounds to the

MALDI-ToF-MS peaks in Table S2 confirm that reactions contributing to cross-linking directly between tannin and soy protein do occur. It confirms also that their interaction is not only based on the classical protein tanning reaction like in leather making thought to be based exclusively on secondary forces interactions between the two materials (Ghahri et al., 2018a; Ghahri and Pizzi, 2018; Ghahri et al., 2018b). Moreover, depending from the condition of reaction also coupling by ionic bonds between $-NH_3^+$ of the protein and the phenolic $-O^-$ of the tannin as shown already for both condensed and hydrolysable tannins (Ghahri et al., 2018a; Ghahri and Pizzi, 2018; Ghahri et al., 2018b).

[Table 2 near here]

3.3.2 Fourier transform infrared (FT-IR) spectroscopy

The FT-IR spectra of pristine SPI, raw tannin, and the reaction product of tannin and SPI are shown in Figure 2. In region I of Figure 2 (d), a broad absorption band approximately 3400 cm^{-1} is related to the characteristic peak of free and bound -NH- or/and -OH groups (Liu et al., 2017; Wang et al., 2017). The hydrogen bonds could be formed between -NH- or/and -OH groups and the carbonyl groups of protein-peptide linkages (Wang et al., 2017). Furthermore, an adsorption peak at 2925 cm^{-1} (region II) can be seen, which is ascribed to symmetric and asymmetric stretching vibrations in $-CH_2/-CH_3$ groups (Chen et al., 2020b). In addition, the SPI characteristic peaks, such as 1635 cm^{-1}, 1515 cm^{-1}, and 1235 cm^{-1} (Figure 2(e)), which are attributed to C=O stretching (amide I), -NH- deformation (amide II), and -CN- stretching and -NH- vibration (amide III), respectively (Wang et al., 2017). The peaks 1391 cm^{-1} (-COO-), 1235 cm^{-1} (amide III), and 1044 cm^{-1} (-C-O-) of SPI disappeared after reacting with tannin, which is assigned to the reaction between SPI and tannin. Furthermore, in Figure 2 (e), there are indications that reactions occur through the primary amines in SPI by forming secondary amines, this being indicated by the two characteristic peaks at 1333 cm^{-1} and 1292 cm^{-1}. The esterification of the tannin hydroxyls by the protein side-chain acids is demonstrated by the 1735 cm^{-1} shoulder. These bands appear to support the MALDI-ToF-MS results that both the reaction of the protein with the flavonoid units of the tannin can occur either through the amino group of a protein side chain or by esterification with the acid group of a side chain of the protein.

[Figure 2 near here]

3.3 Physical and mechanical properties

The physical and mechanical properties of TFS and LTFS foams were determined and are summarized in Table 3 and Figure 3. The control sample showed a lower density, 83.5 kg/m^3, which is similar to literature-reported values of conventional tannin-furanic-formaldehyde foams (Celzard et al., 2010; Tondi et al., 2009b). The tannin-furanic-formaldehyde foam exhibited high brittleness, and the pulverization ratios was 13.68%, because of their lower cross-linking densities and/or their incomplete solidification behaviors. Generally, low density tannin-furanic-formaldehyde foams shows a large mass-loss when gently touched or frictioned it (Li et al., 2021) unless some special arrangements are made (Rangel et al., 2016). The densities of TFS foams were higher than the control, around 94.4 – 112.5 kg/m^3. This result is related to the increased viscosity of the foaming precursor mixture (Table 3). The strong gelation ability of SPI along with the reaction of tannin and SPI can rapidly increase the viscosity of the foaming precursor, even with a small addition of it. Therefore, higher viscosity seems to be a disadvantage for raw materials homogeneous mixing, as well as for bubble formation and volume expansion, resulting in a higher density than the control. This is also found for phenolic foams manufacturing (Jing et al., 2014; Yang et al., 2014; Yang et al., 2013). Additionally, the pulverization ratios (Table 3) of TFS foams had a lower value, only reaching 2.64% to 4.83%. This result is probably because of the higher densities of TFS foams, resulting in a lower brittleness than the control sample. Besides, the covalent cross-linking of tannin with SPI contributes to decrease brittleness. With the introduction of lignin, the foam densities decreased slightly (93.8 – 99.6 kg/m^3) compared to TFS foams. One reason for this phenomenon is the larger cells of the lignin-modified TFS foams, which can be observed from their morphology. The larger cells obtained were probably due to the cell nucleation being affected by lignin addition during the foam preparation (Dolomanova et al., 2011; Xue et al., 2014). Besides, a small amount of lignin reduced the viscosity of the foaming precursor (Table 3) due to the high dispersion and wettability, resulting in lower densities for LTFS than for TFS foams. Therefore, the pulverization ratios increased, as summarized in Table 3.

Figure 3 (a) shows the morphological characteristics of the control, TFS, and LTFS foams. As expected, a closed cell structure with many “pores”, regular cellular structure, and a smooth

cellular surface were obtained, as previously reported (Pizzi, 2019; Wu et al., 2020; Zhou et al., 2019). Nevertheless, the TFS and LTFS cellular structures exhibited larger, inhomogeneous, and rough surface performance compared to the control sample. The major reason for this phenomenon is that the homogenous cellular structure was squeezed in the direction perpendicular to the foam growth because of the slightly shrinkage of foam blocks after the foam reached maximal expansion showing a marked anisotropy. Therefore, some elliptical foam cells can be seen in Figure 3 (a). The cell walls were squeezed and then some wrinkles formed on the surface. For lignin-modified LTFS foams, relatively larger cells were observed than for the control and the TFS samples. This was because the cell nucleation process was influenced by lignin addition (Xue et al., 2014). Therefore, fewer foam nuclei would entrap more blowing gas, leading to a larger cell structure and lower density (Li et al., 2017). As shown in Figure 3 (a) and (b), some clear particles are noticeable on the surface of LTFS foams, but are not visible on the surface of control and TFS foams. The numbers of particles increased with gradually increasing lignin additions. This indicates that lignin can form a protective layer on the surface of the foams as it can be converted to a carbon char layer when in a fire. These particles are one of the factors providing better fire resistance for LTFS than TFS foams.

Figure 3 (c) and (d) show the compressive stress-strain curves and values of control, TFS, and LTFS foams when undergoing a compressive load. The multi-stage deformation observed is consistent with several studies on polymer foams (Chen et al., 2020b; Chen et al., 2020c; Gao et al., 2021; Wu et al., 2020). When comparing TFS and control foams, the compression strength of TFS foams was higher than the control. This can be attributed to the increased density of TFS foams. Moreover, as shown in Table 2, the specific compressive strength increases with the SPI amount. This result indicates that the improved compression strength of TFS foams is not only influenced by the density but also related to the stronger foam cell wall structure resulting from the greater crosslinking between tannin and SPI. Also, the physical enwind between tannin and long chains SPI can promote the improvement of cell wall intensity. The LTFS foams exhibit a lower compression strength than TFS, but similar to that of the control foam. Its less densities are the one of mainly factors for this result. Moreover, the compressive strength possesses the same trend in foam densities, which suggests that the foam density is not the only factor for the

compression strength. The existence of lignin can influence the crosslinking of tannin and SPI which is likely to decrease the strength of the cell wall. In addition, the lager cell structures for LTFS than TFS foams reduced the supporting capacity within the unit pressure range, which were attribute to the reduced cell struts (Li et al., 2021).

[Table 3 near here]

[Figure 3 near here]

3.4 Evaluation of thermal conductivity and thermal stability

The thermal conductivity of the control, TFS, and LTFS foams were evaluated by the hot plate method and the results are shown in Figure 4 (a). The control sample displayed the lowest thermal conductivity, only 0.0391 W/m·K, lower than from other studies of tannin-furanic-formaldehyde foams (Wu et al., 2020; Zhou et al., 2019). The TFS foams had a higher thermal conductivity value, from 0.0431 W/m·K for TFS1 to 0.0442 W/m·K for TFS4 than the control sample, and increasing trend with the increase of SPI. This result probably is attributed to changes in foams density, in general, the higher density will have a higher thermal conductivity (Pizzi, 2019; Szczurek et al., 2014; Tondi and Pizzi, 2009). In parallel, the non-homogenous cell structures (as shown in SEM results) from TFS foams improved their thermal conductivity. Cell morphology can influence the thermal conductivity of polymer foams which as reported by previous study (Li et al., 2021). Lignin-modified LTFS samples had a lowered thermal conductivity value, from 0.04198 W/m·K for L0.5TFS3 to 0.0425 W/m·K for L1.5TFS3, lower than TFS foams but higher than the control. One of the most obvious changes in the lignin-modified TFS foams was the lower foam density. Therefore, this change can directly lead to the decreased thermal conductivity of LTFS foams. Moreover, by comparing TFS and control samples, the uneven morphology and structure of the cells of the former is the reason that it can achieve a higher thermal conductivity than the latter even at similar foam density. For TFS and LTFS foams in this study, the thermal conductivity was higher than the control, still presenting a better performance compared to other insulating materials, thus indicating their outstanding thermal insulation properties.

The thermal stability of the control, TFS, and LTFS foams was studied by thermogravimetric analysis under air conditions. The TG and DTG curves were obtained and are shown in Figure 4

(b) and (c), respectively, and the corresponding data are listed in Table 4. For the control sample, the first weight-loss stage appeared at a temperature range of 25 – 150°C, which is ascribed to the evaporation of the residual blowing agent as well as of absorbed water (Chen et al., 2020b; Li et al., 2019; Wu et al., 2020). The second prominent weight loss (38.14%, as shown in Table 4) stage occurred between 150 – 500°C because of the degradation of the polymer chain forming small molecules (Wu et al., 2020). For instance, the basic structure of soy protein cleaves and decomposes from 250 – 350°C (Liu et al., 2011). The aromatic skeleton of lignin and tannin has better thermal stability, however, thermolysis will occur when the temperature is above 450°C (Chen et al., 2020b; Li et al., 2019; Xue et al., 2014; Zhang et al., 2017). The last one abrupt weight loss (51.33%, as shown in Table 4) occurred when the temperature was above 500°C from pyrolysis of the residual compounds, such as carbon-based char from the second stage (Chen et al., 2020b). These carbon-based compounds formed and covered on the surface of the polymer, thus isolating it from the air and improving the thermal stability of materials. The complete pyrolysis of the control foam, with ~96% weight loss, occurred when the temperature increased to 790°C, resulting in thermally-stable char residues (4.59%, as shown in Table 4).

For the TFS foams, the thermal degradation temperature peaks of the second and third stages were higher than the control, as shown in Table 4. This is related to the stable and compact crosslinked structure between tannin and SPI (Ghahri et al., 2018a; Ghahri and Pizzi, 2018; Ghahri et al., 2018b). The final thermally-stable char residues reached 37.16% at 4 g SPI addition, but only 5.15% at 1 g SPI addition, which was still higher than the control. Hence, such high final residues of TFS foams indicated that the SPI substitution for formaldehyde increased char formation and improved thermal stability. As for the lignin addition, from the DTG curves, it can be seen that the initial and second thermal degradation temperature peaks presented a similar trend with the TFS foams. The degradation temperature peak in the third stage appears to have shifted from ~640°C to ~770°C, as shown in Table 4. Therefore, this phenomenon can show that the high carbon content lignin improved the formation of thermally-stable char (carbonization) (Kong et al., 2018). Moreover, its final mass residue has increased by introducing of lignin, approximately 38–43%. Hence, the thermal stability of TFS foams can further be improved by lignin.

[Figure 4 near here]

[Table 4 near here]

3.5 Evaluation of flame-retardant properties

The flame resistance of the control, TFS, and LTFS samples was evaluated by measuring the limiting oxygen index (LOI) and the results are shown in Figure 5a. As expected, the LOI of a typical tannin-furanic-formaldehyde foam, i.e., the control sample in this work, is 29.37%, indicating it is a flame-retardant material (Zhou et al., 2019). The SPI-substituted TFS samples had higher LOI values, from 38.17% to 40.37%, when the SPI replacement addition was from 1 g to 4 g, 29.96–37.45% higher than the control sample. This effect can be ascribed to the closed-cell morphology structure of TFS and LTFS foams. SEM images (Figure 3) show that closed-cell structures with many "pores" are in the control sample. The air can then circulate in the foam interior through these opened pores, thereby providing a more suitable environment for combustion (Li et al., 2019). Conversely, the TFS and LTFS foams relatively closed-cell structures block the air exchange between the inside and outside of the foam cells, acting as a flame retardant.

Lignin-modified TFS samples (LTFS) have a higher LOI value than TFS foams (Figure 5). The LOI value of L0.5TFS3 is 40.5% which increased to 41.33% with 1.5 g lignin addition (L1.5TFS3). These results indicated that lignin contributed to the flame-retardant performance of LTFS foams. Its high carbon-containing polyphenol structure contributes to higher char carbon productivity at higher temperatures (Chen et al., 2020b; Wu et al., 2020; Yang et al., 2012). Hence, the char covering layer further obstructs contact of the combustion interface with the air, thereby protecting the materials (Yang et al., 2012). However, the LOI value is lower with 2 g lignin (40.83%). This decreased in the LOI value for L2TFS3 is attributed to the inflammability of lignin when applied in larger amounts.

Cone calorimetry was used to simulate and evaluate the combustion behavior of the control, TFS3, and L1.5TFS3 samples in a real fire scenario under a constant heat flux of 35 kW/m^2 from a conical heater. The legible peaks of the heat-release rate (PHRR) flaming combustion for the control and TFS3 foams are shown in Figure 5(b). This peak is attributed to the oxidation reaction of volatile pyrolysis substances in the high-temperature environment (Kong et al., 2018).

For TFS, the maximum peak value was significantly lower than the control. In parallel, as shown in Figure 5(c), the TFS foam had a lower THR value than the control. These results indicate that the TFS foams have better flame-retardancy than the control. A valley characterizes the HRR curves which means the char layer protected the materials as combustion continued. The HRR curves increased, thereafter maintaining a stable level longer than 2000 s. No strong flame was observed when the foams were put on the butane torch. These foams are then self-extinguishing after the flame is removed from the sample surface, as shown in Figure S2 and Video S1.

For the L1.5TFS3 sample, the initial peak disappeared and the curve merged in the exothermic phase. Compared to the TFS foam, a lower THR value (Table 5) was obtained which indicated that as the lignin was introduced, the flame-retardant properties of LTFS improved. This was because of the high char production performance of lignin in the high-temperature environment. It covers the surface of materials and forms a barrier of further contact between air and the combustion interface, enhancing the flame-retardancy of TFS foams.

The values of this peak reached 19.49 to 42.16 kW/m^2 (Table 5), lower than most other foams, such as PU foams (Cao et al., 2019; Rao et al., 2018) or wood-based materials (Kong et al., 2018). These results indicated that these foams have lower HRR, better than others that have been developed. Apart from the HRR, the release of smoke (especially CO) also influences the quality of the safety of the material when in a fire (Kong et al., 2018). The control sample exhibited the highest TSP value (Table 5), and after the modification of foam preparation, the novel biomass TFS and LTFS had a lower TSP value. This further indicated that the fire retardancy of TFS and LTFS was better than that of the control sample. The residue trend of all samples can be seen in the TGA results. For Figure 5(d), the control sample almost lost its original shape, turning to a fragile condition after burning. The TFS3 and L1.5TFS3 preserved their original shapes better, with the latter performing best. This feature is particularly important for materials in a fire.

[Figure 5 near here]

[Table 5 near here]

3.6 Formaldehyde emission

To examine if the foams are environment-friendly, formaldehyde emission tests were conducted

and the results are listed in Table 6. As expected, the control sample released the most formaldehyde, two times that of TFS3 and L1.5TFS3. This indicates that the final tannin-furanic-formaldehyde foam released free formaldehyde despite this also being released during the foam curing process. Yet, the formaldehyde emission of the control sample was still lower than the relevant standard requirement. The TFS and LTFS foams do not utilize formaldehyde, avoiding the release of free-formaldehyde. Thus, the application of soybean protein resources was expanded in this study as a substitute for a toxic substance. In short, these novel biomass foams have many improved properties suggesting a wide of industrial production and application prospects.

[Table 6 near here]

4 Conclusions

High biomass, environment-friendly, and flame retardant TFS foams were developed in this study. Mechanical properties, thermal performance, and flame retardancy were measured by substituting SPI for formaldehyde.

The main results obtained were:

(1) A strong crosslinking reaction between tannin and SPI, yielding closed cells foam structures, thus enhancing mechanical properties, reducing pulverization ratios, and improving thermal conductivity (approximately 0.042–0.044 W/m·K) of the modified tannin foams as well as yielding a better thermal stability.

(2) The increased LOI value, a lower heat-release rate, and increased char residue were obtained. The TFS foams exhibited strong flame retardancy and suppressed smoke generation while undergoing combustion.

(3) Lignin addition decreased the crosslinking of tannin and SPI, increased foam cell size, thereby altering the mechanical properties of TFS foams. The addition of lignin further improved the thermal stability of TFS foams, along with a lower heat-release rate and lower smoke production. This indicates that LTFS enhanced flame retardancy more than that of TFS.

(4) The low formaldehyde emission confirms the good environmental performance of these novel biomass foams. Such novel sustainable TFS foams have thus a good potential for industrial

473 application.

474 **5 Acknowledgement**

475 This work was supported by National Natural Science Foundation of China (NSFC 31760187,
476 31971595), Yunnan Provincial Natural Science Foundation (2017FB060), the “Ten-thousand
477 Program”-youth talent support program and Yunnan Provincial Reserve Talents for Middle &
478 Young Academic and Technical Leaders (2019HB026), Scholarship from China Scholarship
479 Council (CSC), Yunnan Provincial Key Laboratory of Wood Adhesives and Glued Products. The
480 LERMAB is supported by a grant of the French Agence Nationale de la Recherche (ANR) as
481 part of the laboratory of excellence (LABEX) ARBRE.

482 **6 References**

483 Abdullah, U.H.B., Pizzi, A., 2012. Tannin-furfuryl alcohol wood panel adhesives without
484 formaldehyde. Eur. J. Wood Wood. Prod., 71, 131-132. DOI:
485 10.1007/s00107-012-0629-4.

486 Basso, M., Lacoste, C., Pizzi, A., Fredon, E., Delmotte, L., 2014a. Flexible tannin-furanic films
487 and lacquers. Ind. Crops Prod., 61, 352-360. DOI: 10.1016/j.indcrop.2014.07.019.

488 Basso, M.C., Giovando, S., Pizzi, A., Celzard, A., Fierro, V., 2013. Tannin/furanic foams without
489 blowing agents and formaldehyde. Ind. Crops Prod., 49, 17-22. DOI:
490 10.1016/j.indcrop.2013.04.043.

491 Basso, M.C., Giovando, S., Pizzi, A., Pasch, H., Pretorius, N., Delmotte, L., Celzard, A., 2014b.
492 Flexible-elastic copolymerized polyurethane-tannin foams. J. Appl. Polym. Sci., 131. DOI:
493 10.1002/app.40499.

494 Basso, M.C., Li, X., Fierro, V., Pizzi, A., Giovando, S., Celzard, A., 2011. Green,
495 formaldehyde-free, foams for thermal insulation. Adv. Mater. Lett, 2, 378-382. DOI:
496 10.5185/amlett.2011.4254.

497 Basso, M.C., Pizzi, A., 2017. New closed-and open-cell, aldehyde-free protein foams. J.
498 Renewable Mater., 5, 48-53. DOI: 10.7569/JRM.2016.634124.

499 Basso, M.C., Pizzi, A., Delmotte, L., 2015. A new approach to environmentally friendly protein
500 plastics and foams. BioResources, 10, 8014-8024. DOI : 10.15376/biores.10.4.8014-8024.

501 Braghiroli, F., Fierro, V., Pizzi, A., Rode, K., Radke, W., Delmotte, L., Parmentier, J., Celzard, A.,

2013. Reaction of condensed tannins with ammonia. Ind. Crops Prod., 44, 330-335. DOI: 10.1016/j.indcrop.2012.11.024.

Cao, N., Fu, Y., He, J., 2007. Preparation and physical properties of soy protein isolate and gelatin composite films. Food Hydrocolloids, 21, 1153-1162. DOI: 10.1016/j.foodhyd.2006.09.001.

Cao, Z.J., Liao, W., Wang, S.X., Zhao, H.B., Wang, Y.Z., 2019. Polyurethane foams with functionalized graphene towards high fire-resistance, low smoke release, superior thermal insulation. Chem. Eng. J., 361, 1245-1254. DOI: 10.1016/j.cej.2018.12.176.

Celzard, A., Fierro, V., Amaral-Labat, G., Pizzi, A., Torero, J., 2011. Flammability assessment of tannin-based cellular materials. Polym. Degrad. Stab., 96, 477-482. DOI: 10.1016/j.polymdegradstab.2011.01.014.

Celzard, A., Zhao, W., Pizzi, A., Fierro, V., 2010. Mechanical properties of tannin-based rigid foams undergoing compression. Mat. Sci. Eng A-Struct., 527, 4438-4446. DOI: 10.1016/j.msea.2010.03.091.

Chen, X., Guigo, N., Pizzi, A., Sbirrazzuoli, N., Li, B., Fredon, E., Gerardin, C., 2020a. Ambient Temperature Self-Blowing Tannin-Humins Biofoams. Polymers, 12, 2732. DOI: 10.3390/polym12112732.

Chen, X., Li, J., Xi, X., Pizzi, A., Zhou, X., Fredon, E., Du, G., Gerardin, C., 2020b. Condensed tannin-glucose-based NIPU bio-foams of improved fire retardancy. Polym. Degrad. Stab., 175, 109121. DOI: 10.1016/j.polymdegradstab.2020.109121.

Chen, X., Xi, X., Pizzi, A., Fredon, E., Zhou, X., Li, J., Gerardin, C., Du, G., 2020c. Preparation and Characterization of Condensed Tannin Non-Isocyanate Polyurethane (NIPU) Rigid Foams by Ambient Temperature Blowing. Polymers, 12, 750. DOI: 10.3390/polym12040750.

Chiou, B.-S., Cao, T., Bilbao-Sainz, C., Vega-Galvez, A., Glenn, G., Orts, W., 2020. Properties of gluten foams containing different additives. Ind. Crops Prod., 152, 112511. DOI: 10.1016/j.indcrop.2020.112511.

Dolomanova, V., Rauhe, J.C.M., Jensen, L.R., Pyrz, R., Timmons, A.B., 2011. Mechanical properties and morphology of nano-reinforced rigid PU foam. J. Cell. Plast., 47, 81-93. DOI:

10.1177/0021955X10392200.

Frihart, C.R., Lorenz, L.F., 2019. Specific oxidants improve the wood bonding strength of soy and other plant flours. J. Polym. Sci., Part A: Polym. Chem., 57, 1017-1023. DOI: 10.1002/pola.29357.

Frihart, C.R., Pizzi, A., Xi, X., Lorenz, L.F., 2019. Reactions of Soy flour and Soy protein by non-volatile aldehydes generation by specific oxidation. Polymers, 11, 1478. DOI: 10.3390/polym11091478.

Gao, C., Li, M., Zhu, C., Hu, Y., Shen, T., Li, M., Ji, X., Lyu, G., Zhuang, W., 2021. One-pot depolymerization, demethylation and phenolation of lignin catalyzed by HBr under microwave irradiation for phenolic foam preparation. Compos. Part B-eng., 205, 108530. DOI: 10.1016/j.compositesb.2020.108530.

Ghahri, S., Mohebby, B., Pizzi, A., Mirshokraie, A., Mansouri, H.R., 2018a. Improving water resistance of soy-based adhesive by vegetable tannin. J. Polym. Environ., 26, 1881-1890. DOI: 10.1007/s10924-017-1090-6.

Ghahri, S., Pizzi, A., 2018. Improving soy-based adhesives for wood particleboard by tannins addition. Wood Sci. Technol., 52, 261-279. DOI: 10.1007/s00226-017-0957-y.

Ghahri, S., Pizzi, A., Mohebby, B., Mirshokraie, A., Mansouri, H.R., 2018b. Soy-based, tannin-modified plywood adhesives. J. Adhes., 94, 218-237. DOI: 10.1080/00218464.2016.1258310.

Gu, W., Liu, X., Li, F., Shi, S.Q., Xia, C., Zhou, W., Zhang, D., Gong, S., Li, J., 2019. Tough, strong, and biodegradable composite film with excellent UV barrier performance comprising soy protein isolate, hyperbranched polyester, and cardanol derivative. Green Chem., 21, 3651-3665. DOI: 10.1039/C9GC01081E.

Guo, Y., Zhang, X., Hao, W., Xie, Y., Chen, L., Li, Z., Zhu, B., Feng, X., 2018. Nano-bacterial cellulose/soy protein isolate complex gel as fat substitutes in ice cream model. Carbohydr. Polym., 198, 620-630. DOI: 10.1016/j.carbpol.2018.06.078.

Jahanshahi, S., Pizzi, A., Abdulkhani, A., Doosthoseini, K., Shakeri, A., Lagel, M., Delmotte, L., 2016. MALDI-TOF, ^{13}C NMR and FT-MIR analysis and strength characterization of glycidyl ether tannin epoxy resins. Ind. Crops Prod., 83, 177-185. DOI:

10.1016/j.indcrop.2015.11.067.

Jana, P., Fierro, V., Pizzi, A., Celzard, A., 2015. Thermal conductivity improvement of composite carbon foams based on tannin-based disordered carbon matrix and graphite fillers. Mater. Des., 83, 635-643. DOI: 10.1016/j.matdes.2015.06.057.

Jing, S., Li, T., Li, X., Xu, Q., Hu, J., Li, R., 2014. Phenolic foams modified by cardanol through bisphenol modification. J. Appl. Polym. Sci., 131. DOI: 10.1002/app.39942.

Kong, L., Guan, H., Wang, X., 2018. In Situ Polymerization of Furfuryl Alcohol with Ammonium Dihydrogen Phosphate in Poplar Wood for Improved Dimensional Stability and Flame Retardancy. ACS Sustainable Chem. Eng., 6, 3349-3357. DOI: 10.1021/acssuschemeng.7b03518.

Lacoste, C., Basso, M., Pizzi, A., Celzard, A., Laborie, M., 2015. Natural albumin/tannin cellular foams. Ind. Crops Prod., 73, 41-48. DOI: 10.1016/j.indcrop.2015.03.087.

Lacoste, C., Basso, M.C., Pizzi, A., Laborie, M.-P., Garcia, D., Celzard, A., 2013. Bioresourced pine tannin/furanic foams with glyoxal and glutaraldehyde. Ind. Crops Prod., 45, 401-405. DOI: 10.1016/j.indcrop.2012.12.032.

Li, B., Wang, Y., Mahmood, N., Yuan, Z., Schmidt, J., Xu, C., 2017. Preparation of bio-based phenol formaldehyde foams using depolymerized hydrolysis lignin. Ind. Crops Prod., 97, 409-416. DOI: 10.1016/j.indcrop.2016.12.063.

Li, J., Liao, J., Essawy, H., Zhang, J., Li, T., Wu, Z., Du, G., Zhou, X., 2021. Preparation and characterization of novel cellular/nonporous foam structures derived from tannin furanic resin. Ind. Crops Prod., 162, 113264. DOI: 10.1016/j.indcrop.2021.113264.

Li, J., Zhang, A., Zhang, S., Gao, Q., Zhang, W., Li, J., 2019. Larch tannin-based rigid phenolic foam with high compressive strength, low friability, and low thermal conductivity reinforced by cork powder. Composites. Part B, 156, 368-377. DOI: 10.1016/j.compositesb.2018.09.005.

Li, X., Basso, M., Fierro, V., Pizzi, A., Celzard, A., 2012a. Chemical modification of tannin/furanic rigid foams by isocyanates and polyurethanes. Maderas. Ciencia y tecnología, 14, 257-265. DOI : 10.4067/S0718-221X2012005000001.

Li, X., Essawy, H., Pizzi, A., Delmotte, L., Rode, K., Le Nouen, D., Fierro, V., Celzard, A.,

2012b. Modification of tannin based rigid foams using oligomers of a hyperbranched poly (amine-ester). J. Polym. Res., 19, 1-9. DOI: 10.1007/s10965-012-0021-4.

Li, X., Pizzi, A., Cangemi, M., Fierro, V., Celzard, A., 2012c. Flexible natural tannin-based and protein-based biosourced foams. Ind. Crops Prod., 37, 389-393. DOI: 10.1016/j.indcrop.2011.12.037.

Li, X., Pizzi, A., Cangemi, M., Navarrete, P., Segovia, C., Fierro, V., Celzard, A., 2012d. Insulation rigid and elastic foams based on albumin. Ind. Crops Prod., 37, 149-154. DOI: 10.1016/j.indcrop.2011.11.030.

Li, X., Srivastava, V., Pizzi, A., Celzard, A., Leban, J., 2013. Nanotube-reinforced tannin/furanic rigid foams. Ind. Crops Prod., 43, 636-639. DOI: 10.1016/j.indcrop.2012.08.008.

Liang, J., Wu, Z., Lei, H., Xi, X., Li, T., Du, G., 2017. The Reaction between Furfuryl Alcohol and Model Compound of Protein. Polymers, 9, 711. DOI: 10.3390/polym9120711.

Liu, B., Jiang, L., Zhang, J., 2011. Extrusion Foaming of Poly (lactic acid)/Soy Protein Concentrate Blends. Macromol. Mater. Eng., 296, 835-842. DOI: 10.1002/mame.201000449.

Liu, C., Zhang, Y., Li, X., Luo, J., Gao, Q., Li, J., 2017. “Green” bio-thermoset resins derived from soy protein isolate and condensed tannins. Ind. Crops Prod., 108, 363-370. DOI: 10.1016/j.indcrop.2017.06.057.

Liu, H., Li, C., Sun, X.S., 2015. Improved water resistance in undecylenic acid (UA)-modified soy protein isolate (SPI)-based adhesives. Ind. Crops Prod., 74, 577-584. DOI: 10.1016/j.indcrop.2015.05.043.

Ma, X., Chen, W., Yan, T., Wang, D., Hou, F., Miao, S., Liu, D., 2020. Comparison of citrus pectin and apple pectin in conjugation with soy protein isolate (SPI) under controlled dry-heating conditions. Food. Chem., 309, 125501. DOI: 10.1016/j.foodchem.2019.125501.

Meikleham, N., Pizzi, A., 1994. Acid-and alkali-catalyzed tannin-based rigid foams. J. Appl. Polym. Sci., 53, 1547-1556. DOI: 10.1002/app.1994.070531117.

Pizzi, A., 2019. Tannin-based biofoams-A review. J. Renewable Mater., 7, 474-489. DOI: 10.32604/jrm.2019.06511.

Pizzi, A., Tondi, G., Pasch, H., Celzard, A., 2008. Matrix-assisted laser desorption/ionization

time-of-flight structure determination of complex thermoset networks: Polyflavonoid tannin-furanic rigid foams. J. Appl. Polym. Sci., 110, 1451-1456. DOI: 10.1002/app.28545.

Rangel, G., Chapuis, H., Basso, M.-C., Pizzi, A., Delgado-Sanchez, C., Fierro, V., Celzard, A., Gerardin-Charbonnier, C., 2016. Improving water repellence and friability of tannin-furanic foams by oil-grafted flavonoid tannins. Bioresources, 11, 7754-7768. DOI: 10.15376/biores.11.3.7754-7768.

Rao, W.-H., Zhu, Z.-M., Wang, S.-X., Wang, T., Tan, Y., Liao, W., Zhao, H.-B., Wang, Y.-Z., 2018. A reactive phosphorus-containing polyol incorporated into flexible polyurethane foam: Self-extinguishing behavior and mechanism. Polym. Degrad. Stab., 153, 192-200. DOI: 10.1016/j.polymdegradstab.2018.04.029.

Santiago-Medina, F.-J., Pizzi, A., Basso, M.C., Delmotte, L., Celzard, A., 2017. Polycondensation Resins by Flavonoid Tannins Reaction with Amines. Polymers, 9, 37. DOI: 10.3390/polym9020037.

Santiago-Medina, F., Delgado-Sánchez, C., Basso, M., Pizzi, A., Fierro, V., Celzard, A., 2018a. Mechanically blown wall-projected tannin-based foams. Ind. Crops Prod., 113, 316-323. DOI: 10.1016/j.indcrop.2018.01.049.

Santiago-Medina, F., Tenorio-Alfonso, A., Delgado-Sánchez, C., Basso, M., Pizzi, A., Celzard, A., Fierro, V., Sánchez, M., Franco, J., 2018b. Projectable tannin foams by mechanical and chemical expansion. Ind. Crops Prod., 120, 90-96. DOI: 10.1016/j.indcrop.2018.04.048.

Szczurek, A., Fierro, V., Pizzi, A., Stauber, M., Celzard, A., 2014. A new method for preparing tannin-based foams. Ind. Crops Prod., 54, 40-53. DOI: 10.1016/j.indcrop.2014.01.012.

Thébault, M., Pizzi, A., Santiago-Medina, F.J., Al-Marzouki, F.M., Abdalla, S., 2017. Isocyanate-Free Polyurethanes by Coreaction of Condensed Tannins with Aminated Tannins. J. Renewable Mater., 5, 21-29. DOI: 10.7569/JRM.2016.634116.

Tondi, G., Fierro, V., Pizzi, A., Celzard, A., 2009a. Tannin-based carbon foams. Carbon, 47, 1480-1492. DOI: 10.1016/j.carbon.2009.01.041.

Tondi, G., Oo, C., Pizzi, A., Trosa, A., Thévenon, M.-F., 2009b. Metal adsorption of tannin based rigid foams. Ind. Crops Prod., 29, 336-340. DOI: 10.1016/j.indcrop.2008.06.006.

Tondi, G., Pizzi, A., 2009. Tannin-based rigid foams: Characterization and modification. Ind.

Crops Prod., 29, 356-363. DOI: 10.1016/j.indcrop.2008.07.003.

Tondi, G., Pizzi, A., Olives, R., 2008a. Natural tannin-based rigid foams as insulation for doors and wall panels. Maderas. Ciencia y tecnología, 10, 219-227. DOI: 10.4067/S0718-221X2008000300005.

Tondi, G., Pizzi, A., Pasch, H., Celzard, A., Rode, K., 2008b. MALDI-ToF investigation of furanic polymer foams before and after carbonization: Aromatic rearrangement and surviving furanic structures. Eur. Polym. J., 44, 2938-2943. DOI : 10.1016/j.eurpolymj.2008.06.029.

Tondi, G., Zhao, W., Pizzi, A., Du, G., Fierro, V., Celzard, A., 2009c. Tannin-based rigid foams: a survey of chemical and physical properties. Bioresour. Technol., 100, 5162-5169. DOI: 10.1016/j.biortech.2009.05.055.

Wang, Z., Kang, H., Zhang, W., Zhang, S., Li, J., 2017. Improvement of interfacial interactions using natural polyphenol-inspired tannic acid-coated nanoclay enhancement of soy protein isolate biofilms. Appl. Surf. Sci., 401, 271-282. DOI: 10.1016/j.apsusc.2017.01.015.

Wang, Z., Zhao, S., Zhang, W., Qi, C., Zhang, S., Li, J., 2019. Bio-inspired cellulose nanofiber-reinforced soy protein resin adhesives with dopamine-induced codeposition of “water-resistant” interphases. Appl. Surf. Sci., 478, 441-450. DOI: 10.1016/j.apsusc.2019.01.154.

Wu, X., Yan, W., Zhou, Y., Luo, L., Yu, X., Luo, L., Fan, M., Du, G., Zhao, W., 2020. Thermal, morphological, and mechanical characteristics of sustainable tannin bio-based foams reinforced with wood cellulosic fibers. Ind. Crops Prod., 158, 113029. DOI: 10.1016/j.indcrop.2020.113029.

Xi, X., Pizzi, A., Gerardin, C., Chen, X., Amirou, S., 2020. Soy protein isolate-based polyamides as wood adhesives. Wood Sci. Technol., 54, 89-102. DOI: 10.1007/s00226-019-01141-9.

Xiao, Z., Li, Y., Wu, X., Qi, G., Li, N., Zhang, K., Wang, D., Sun, X.S., 2013. Utilization of sorghum lignin to improve adhesion strength of soy protein adhesives on wood veneer. Ind. Crops Prod., 50, 501-509. DOI: 10.1016/j.indcrop.2013.07.057.

Xue, B.-L., Wen, J.-L., Sun, R.-C., 2014. Lignin-Based Rigid Polyurethane Foam Reinforced with Pulp Fiber: Synthesis and Characterization. ACS Sustainable Chem. Eng., 2,

1474-1480. DOI: 10.1021/sc5001226.

Yang, C., Zhuang, Z.-H., Yang, Z.-G., 2014. Pulverized polyurethane foam particles reinforced rigid polyurethane foam and phenolic foam. J. Appl. Polym. Sci., 131. DOI: 10.1002/app.39734.

Yang, H., Wang, X., Yuan, H., Song, L., Hu, Y., Yuen, R.K.K., 2012. Fire performance and mechanical properties of phenolic foams modified by phosphorus-containing polyethers. J. Polym. Res., 19, 9831. DOI: 10.1007/s10965-012-9831-7.

Yang, Z., Yuan, L., Gu, Y., Li, M., Sun, Z., Zhang, Z., 2013. Improvement in mechanical and thermal properties of phenolic foam reinforced with multiwalled carbon nanotubes. J. Appl. Polym. Sci., 130, 1479-1488. DOI: 10.1002/app.39326.

Zhang, A., Li, J., Zhang, S., Mu, Y., Zhang, W., Li, J., 2017. Characterization and acid-catalysed depolymerization of condensed tannins derived from larch bark. RSC Adv., 7, 35135-35146. DOI: 10.1039/C7RA03410E.

Zhao, S., Wang, Z., Li, Z., Li, L., Li, J., Zhang, S., 2019. Core-shell nanohybrid elastomer based on co-deposition strategy to improve performance of soy protein adhesive. ACS Appl. Mater. Interfaces, 11, 32414-32422. DOI: 10.1021/acsami.9b11385.

Zhao, Y., Wang, Z., Zhang, Q., Chen, F., Yue, Z., Zhang, T., Deng, H., Huselstein, C., Anderson, D.P., Chang, P.R., 2018. Accelerated skin wound healing by soy protein isolate–modified hydroxypropyl chitosan composite films. Int. J. Biol. Macromol., 118, 1293-1302. DOI: 10.1016/j.ijbiomac.2018.06.195.

Zhou, X., Li, B., Xu, Y., Essawy, H., Wu, Z., Du, G., 2019. Tannin-furanic resin foam reinforced with cellulose nanofibers (CNF). Ind. Crops Prod., 134, 107-112. DOI: 10.1016/j.indcrop.2019.03.052.

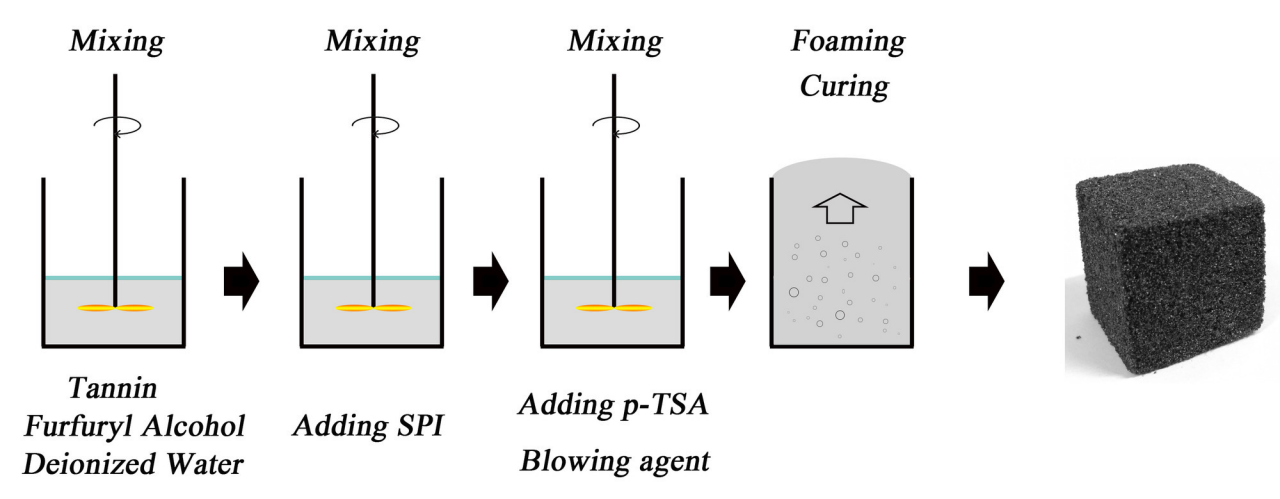
Mixing
Mixing
Mixing
Foaming
Curing
Tannin
Furfuryl Alcohol
Deionized Water
Adding SPI
Adding p-TSA
Blowing agent

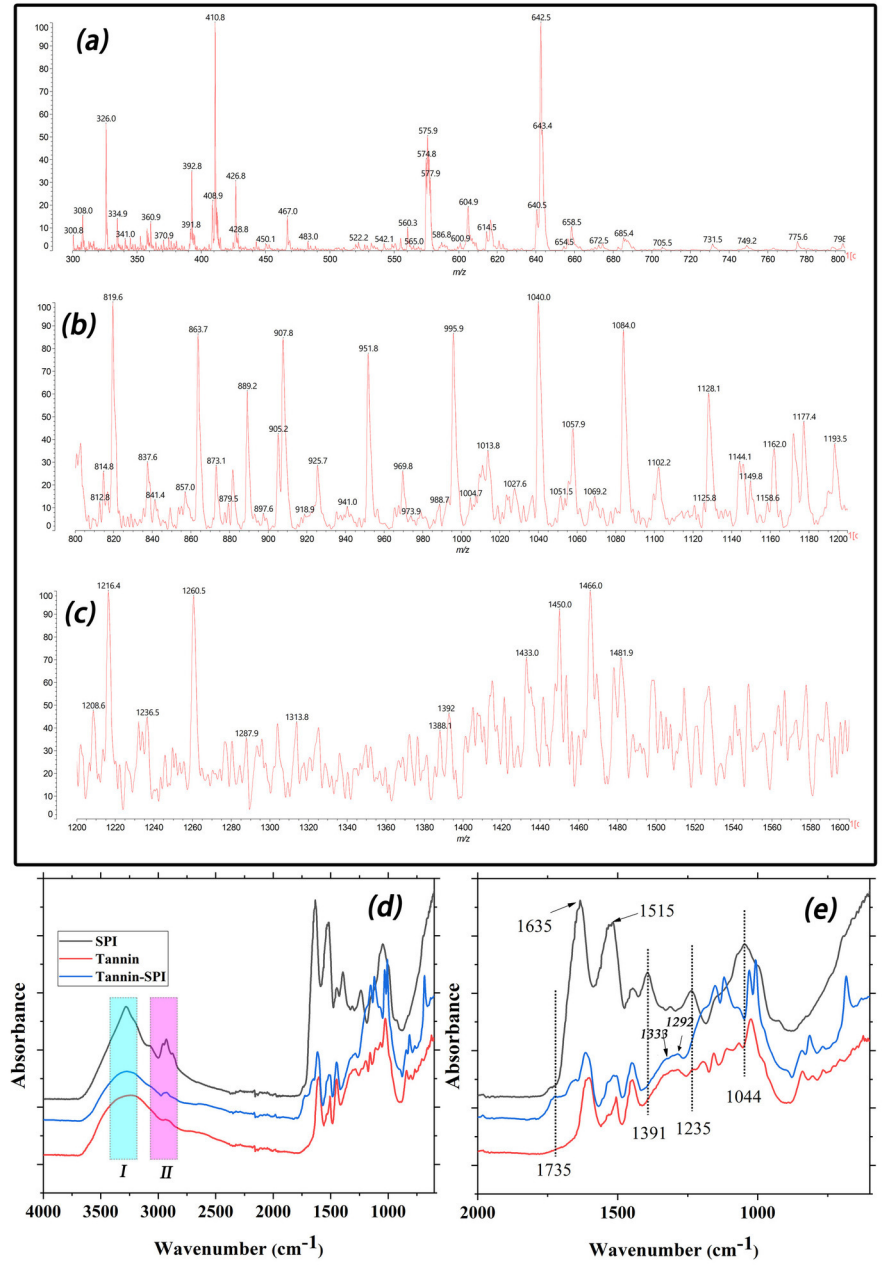
(a)
(b)
(c)
(d)
(e)
m/z
SPI
Tannin
Tannin-SPI
Absorbance
Wavenumber (cm-1)
I
II
1635
1515
1338
1292
1391
1235
1044
1735

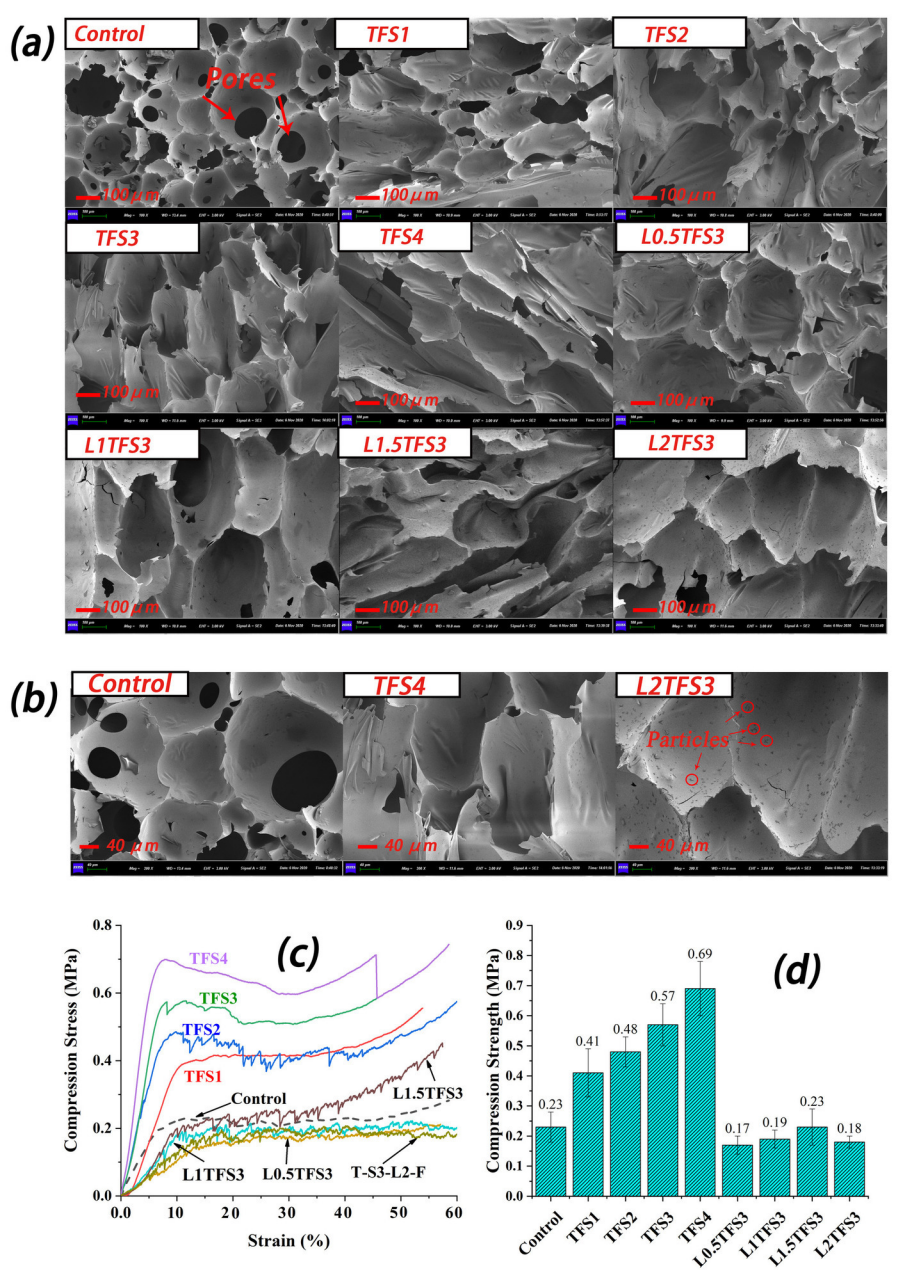
(a)
Control
Pores
TFS1
TFS2
TFS3
TFS4
L0.5TFS3
L1TFS3
L1.5TFS3
L2TFS3
100 μm
(b)
Control
TFS4
L2TFS3
Particles
40 μm
(c)
Compression Stress (MPa)
Strain (%)
TFS4
TFS3
TFS2
TFS1
Control
L1.5TFS3
L1TFS3
L0.5TFS3
T-S3-L2-F
(d)
Compression Strength (MPa)
0.23
0.41
0.48
0.57
0.69
0.17
0.19
0.23
0.18
Control
TFS1
TFS2
TFS3
TFS4
L0.5TFS3
L1TFS3
L1.5TFS3
L2TFS3

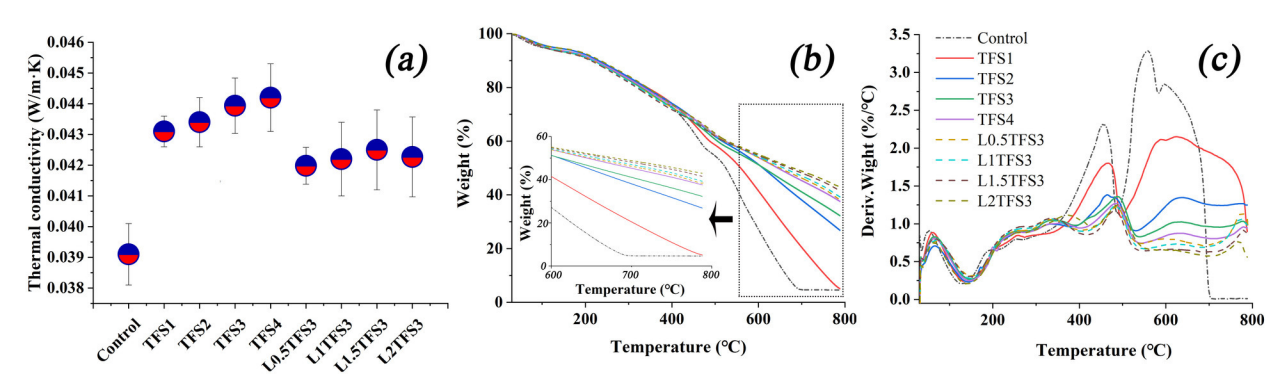
(a)
Thermal conductivity (W/m·K)
0.046
0.045
0.044
0.043
0.042
0.041
0.040
0.039
0.038
Control
TFS1
TFS2
TFS3
TFS4
L0.5TFS3
L1TFS3
L1.5TFS3
L2TFS3
(b)
Weight (%)
100
80
60
40
20
0
200
400
600
800
Temperature (°C)
Weight (%)
60
40
20
0
600
700
800
Temperature (°C)
(c)
Deriv.Wight (%/°C)
3.5
3.0
2.5
2.0
1.5
1.0
0.5
0.0
Control
TFS1
TFS2
TFS3
TFS4
L0.5TFS3
L1TFS3
L1.5TFS3
L2TFS3
200
400
600
800
Temperature (°C)

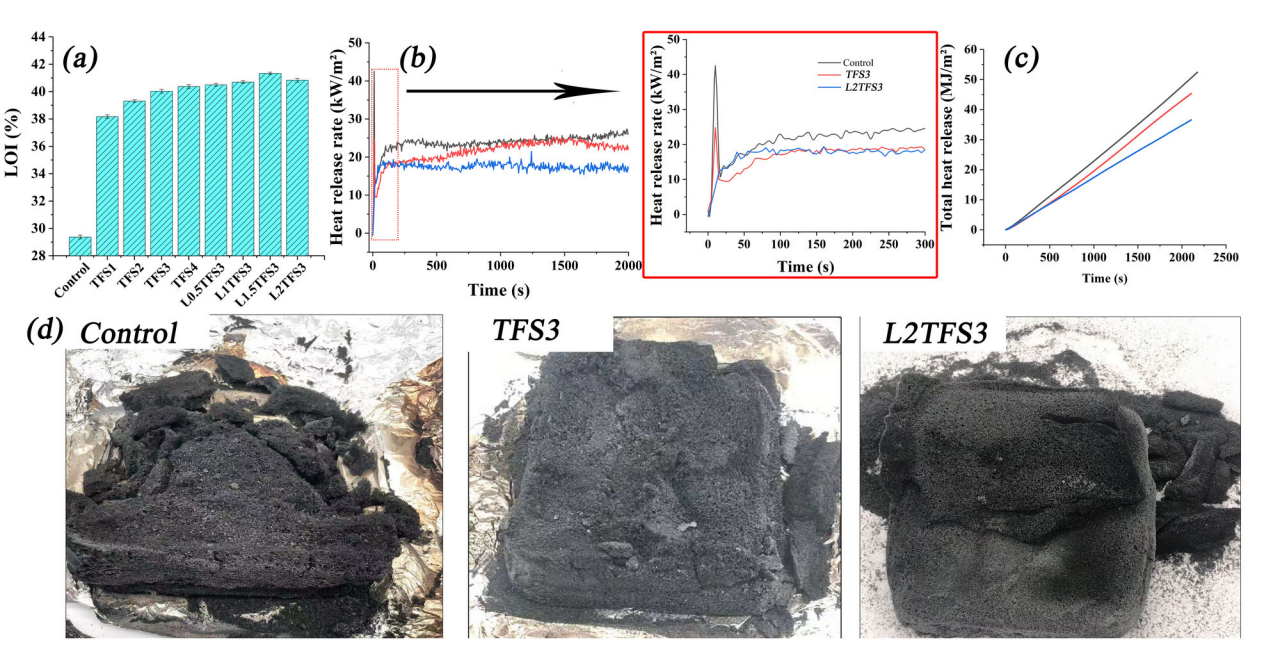
(a)
LOI (%)
Control
TFS1
TFS2
TFS3
TFS4
L0.5TFS3
L1TFS3
L1.5TFS3
L2TFS3
(b)
Heat release rate (kW/m²)
Time (s)
Control
TFS3
L2TFS3
(c)
Total heat release (MJ/m²)
Time (s)
(d)
Control
TFS3
L2TFS3

Table 1 Formulation of series of tannin-SPI-based and tannin-SPI-lignin-based foams

Samples	Tannin (g)	FA (g)	F (g)	SPI (g)	Lignin (g)	Water (g)	p-TSA (g)	DE (g)
Control	30	10.4	7.4			10	12	2.2
TFS1	30	10.4		1		4	12	2.2
TFS2				2				
TFS3				3				
TFS4				4				
L0.5TFS3				3	0.5			
L1TFS3				3	1			
L1.5TFS3				3	1.5			
L2TFS3				3	2			

Table 2 (a) Robinetinidin ***or*** Catechin-Arginine with Na^+; (b) Fisetinidin-Aspartic acid without Na^+; (c) Fisetinidin-Glutamic acid with Na^+; (d) Tryptophan-Aspartic acid-Robinetinidin ***or*** Catechin-Fisetinidin-Arginine-Leucin-Aspartic acid-Tryptophan without Na^+; (e) and (f) Aspartic acid-Robinetinidin ***or*** Catechin-Fisetinidin-Arginine-Leucin-Aspartic acid-Tryptophan without Na^+.

Types	Oligomers
(a)	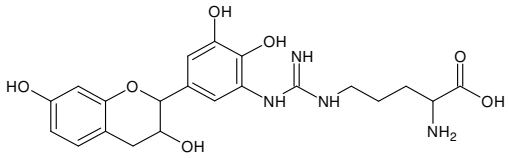
(b)	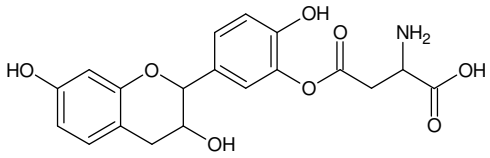
(c)	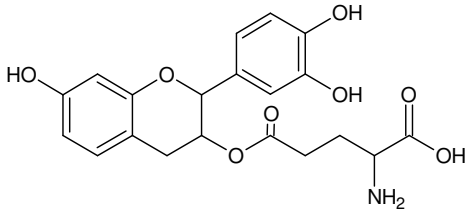
(d)	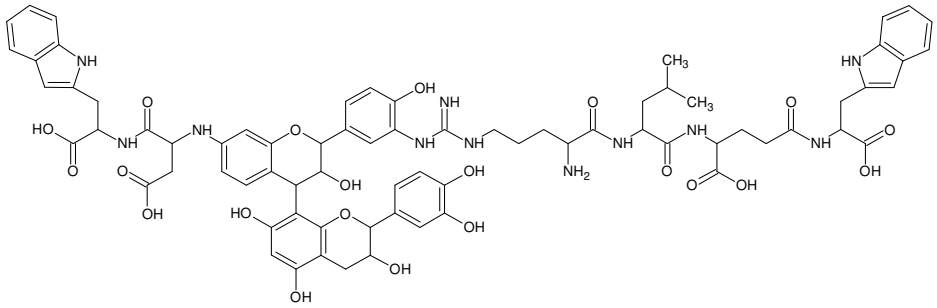
(e)	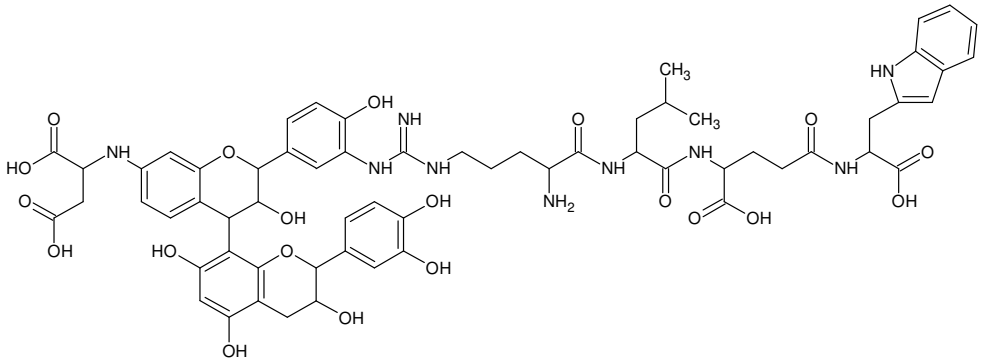

(f)

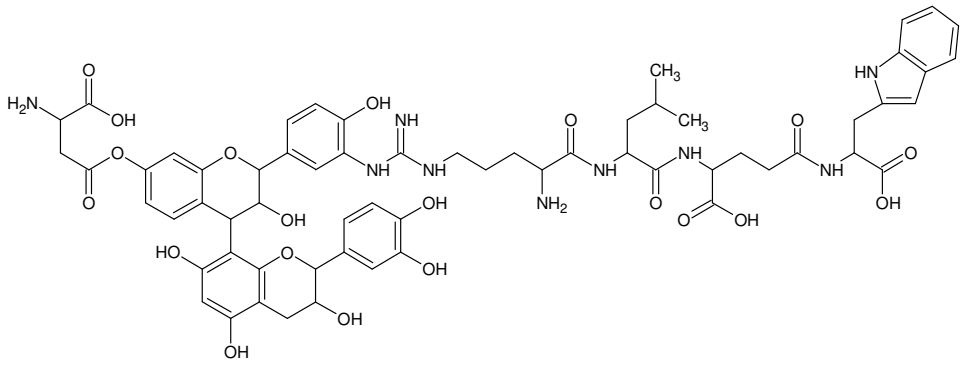
H2N
O
OH
O
O
O
OH
NH
NH
NH
OH
OH
HO
OH
OH
OH
NH2
O
NH
CH3
CH3
NH
O
O
OH
O
NH
HN
O
OH

Table 3 The viscosity of foaming resins, density, pulverization ratios and specific compressive strength of control, TFS, and LTFS foams [a].

Foams	Viscosity (mPa•s)	Density (kg/m^3)	Pulverization ratios (%)	Specific compressive strength ($kPa/kg•m^{-3}$)
Control	2200(35)	83.5(2.5)	13.68(1.03)	2.75
TFS1	17500(145)	94.4(3.1)	4.83(0.72)	4.34
TFS2	27650(221)	98.3(2.6)	4.22(0.49)	4.88
TFS3	35500(187)	108.6(4.8)	3.68(0.21)	5.24
TFS4	48500(180)	112.5(5.5)	2.64(0.38)	6.13
L0.5TFS3	26250(195)	96.5(1.8)	10.01(2.15)	1.76
L1TFS3	32900(207)	98.6(2.1)	8.55(1.12)	1.93
L1.5TFS3	36750(214)	99.6(3.4)	8.24(1.74)	2.31
L2TFS3	40850(224)	93.8(2.2)	11.48(2.21)	1.91

[a]The values in the parentheses are standard deviations

Table 4 TGA data of the control, TFS and LTFS foams.

Foams	T-max[a] (°C)			Weight loss (%)			Residual mass at 790°C (%)
	Step I	Step II	Step III	Step I	Step II	Step III	
Control	52.28	455.64	558.82	5.94	38.14	51.33	4.59
TFS1	61.24	466.59	624.81	5.80	35.17	53.88	5.15
TFS2	63.73	468.72	634.44	5.19	35.70	32.25	26.84
TFS3	65.45	486.21	639.01	6.35	36.21	25.13	32.28
TFS4	64.78	487.81	639.71	6.10	34.79	21.5	37.61
L0.5TFS3	65.73	484.88	774.73	6.18	34.49	20.80	38.52
L1TFS3	66.39	485.53	773.40	5.96	36.03	18.76	39.25
L1.5TFS3	67.38	482.96	772.53	6.57	36.79	15.10	41.54
L2TFS3	65.59	481.35	779.78	5.24	37.27	14.48	43.01

[a] Temperature corresponding to the maximum weight loss rate.

Table 5 Detailed cone calorimetry data of the control, TFS, and LTFS samples [a]

Foams	PHRR [b] (kW/m^2)	THR [b] (MJ/m^2)	TSP [b] (m^2)	Residue [b] (wt %)	Ref.
Control	42.16(2.62)	42.65(2.16)	0.13(0.02)	26.73(1.55)	
TFS3	25.38(2.05)	38.65(1.08)	0.11(0.01)	32.41(2.34)	★[c]
L1.5TFS3	19.49(1.68)	31.57(1.98)	0.05(0.01)	41.34(3.66)	
Wood	167.86(4.06)	68.69(2.29)	2.18(0.28)	-	(Kong et al., 2018)
Wood/PFA	233.21(34.94)	83.36(2.65)	5.37(0.35)	-	
Wood/PFA/ADP	156.61(4.94)	45.10(0.16)	0.22(0.04)	-	
PUF-0	232.7(21)	10.7(2)	5.93(0.6)	-	(Cao et al., 2019)
PUF-EG	207.9(23)	10.1(1.7)	5.36(0.3)	-	
PUF-200	103(13)	5.9(1.0)	2.08(0.2)	-	
Pure FPUF	310(11)	22.5(0.5)	4.51(0.06)	4.3(0.7)	(Rao et al., 2018)

[a] The values in the parentheses are standard deviations;

[b] PHRR, THR, TSP and residue represented the time to ignition, peak heat release rate, total heat release, total smoke production and residue after tests, respectively;

[c] ★ represents this work.

Table 6 Formaldehyde emission of the control, TFS3, and L1.5TFS3 foams [a]

Samples	Formaldehyde emission (mg/m^3)
Control	0.08 (0.02)
TFS3	0.03(0.01)
L1.5TFS3	0.03(0.01)
GB/T 17657-2013	≤0.124

[a] The values in the parentheses are standard deviations

Lignocellulosic Biomass

Hemicellulose

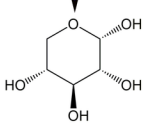

Xylose

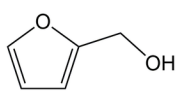

Furfuryl Alcohol (FA)

Extractive

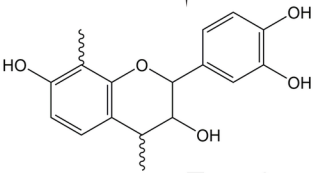

Tannin

Soy Protein Isolate (SPI)

Water+Diethyl ether (DE)

p-toluene-4-sulfonic acid (pTSA)